

Observation of entanglement sudden death and rebirth by controlling solid-state spin bath

F. Wang¹, P.-Y. Hou¹, Y.-Y. Huang¹, W.-G. Zhang¹, X.-L. Ouyang¹, X. Wang¹, X.-Z. Huang¹, H.-L. Zhang¹, L. He¹, X.-Y. Chang¹, L.-M. Duan^{1,2}

¹*Center for Quantum Information, IIIS, Tsinghua University, Beijing 100084, PR China*

²*Department of Physics, University of Michigan, Ann Arbor, Michigan 48109, USA*

Quantum entanglement, the essential resource for quantum information processing, has rich dynamics under different environments. Probing different entanglement dynamics typically requires exquisite control of complicated system-environment coupling in real experimental systems. Here, by a simple control of the effective solid-state spin bath in a diamond sample, we observe rich entanglement dynamics, including the conventional asymptotic decay as well as the entanglement sudden death, a term coined for the phenomenon of complete disappearance of entanglement after a short finite time interval. Furthermore, we observe counter-intuitive entanglement rebirth after its sudden death in the same diamond sample by tuning an experimental parameter, demonstrating that we can conveniently control the non-Markovianity of the system-environment coupling through a natural experimental knob. Further tuning of this experimental knob can make the entanglement dynamics completely coherent under the same environmental coupling. Probing of entanglement dynamics, apart from its fundamental interest, may find applications in quantum information processing through control of the environmental coupling.

Besides its significance as a fundamental concept in quantum mechanics, entanglement has been recognized as an essential resource for quantum computation and communication [1–4]. In any real experimental system, due to its inevitable coupling to the surrounding environment, entanglement degrades with time, leading to various kinds of entanglement dynamics under different environmental couplings [5–9]. The most common one is the asymptotic decay of the entanglement, where the entanglement approaches zero (typically exponentially) as the time goes to infinity. This behavior is similar to the quantum coherence decay and arises when the environmental coupling is dominated by pure dephasing [5, 6]. Under more complicated dissipation, entanglement may completely vanish in a finite (typically short) time interval, a phenomenon called the entanglement sudden death (ESD) [7–11]. The ESD is identified to be more disruptive to quantum information processing due to the fast disappearance of entanglement [7–9]. Under more unusual situations which require non-Markovianity of the system-environment coupling, the entanglement can reappear after its sudden death for a while, which is termed as the entanglement rebirth [9]. The entanglement sudden death and rebirth have been extensively studied theoretically [12–18]. On the experimental side, all-optical quantum experiments can simulate environmental couplings of photonic qubits by linear optics elements to demonstrate the ESD [19, 20] as well as the non-Markovian coupling [21–23]. ESD is also observed between atomic ensembles but with no entanglement rebirth or non-Markovian behavior [24]. It is desirable to find an experimental system where the natural system-environment coupling and its Markovianity can be controlled to probe different kinds of entanglement dynamics in a single system, including the ESD and the entanglement rebirth. Probe of the non-Markovian dynamics plays an important role in control of open quantum systems [25–27].

In this paper, we demonstrate that rich entanglement dynamics can be observed in a single diamond sample by controlling the effective coupling of spin qubits to the solid-state spin bath. The system-environment coupling is controlled by the dynamical decoupling pulses, which provide a tunable filter function to modify the contributing noise spectrum of the bath. Depending on the control parameter in this filter function, we observe the Markovian asymptotic decay as well as the sudden death of the entanglement. Tuning of the same parameter allows us to go to non-Markovian region of the dissipation, where we observe the entanglement rebirth after the ESD. Further tuning of this parameter can make the entanglement dynamics completely coherent under this spin bath, showing entanglement Rabi oscillations.

Our experimental demonstration makes use of the hybrid spin system composed of the electron spin and the host ¹⁴N nuclear spin associated with the nitrogen-vacancy center in diamond (Fig. 1(a)). The surrounding ¹³C nuclear spins in the crystal lattice act as a natural reservoir and are coupled to the electron spin via varying anisotropic hyperfine interactions (Fig. 1(a)). The impact of the ¹³C bath on the nitrogen nuclear spin can be ignored due to the lower interaction strength compared to that of the electron spin.

The experiments are performed at room temperature on a bulk diamond sample with a natural ¹³C abundance. Under an external magnetic field of 479 Gauss along the NV symmetry axis, both the electron and the nitrogen nuclear spin are polarized via optical pumping [28]. We prepare entangled state between the two spins using a rf-induced π rotation of the nuclear spin conditional on the state of the electron spin (Fig. 1(b)). Coherence of the electron spin is

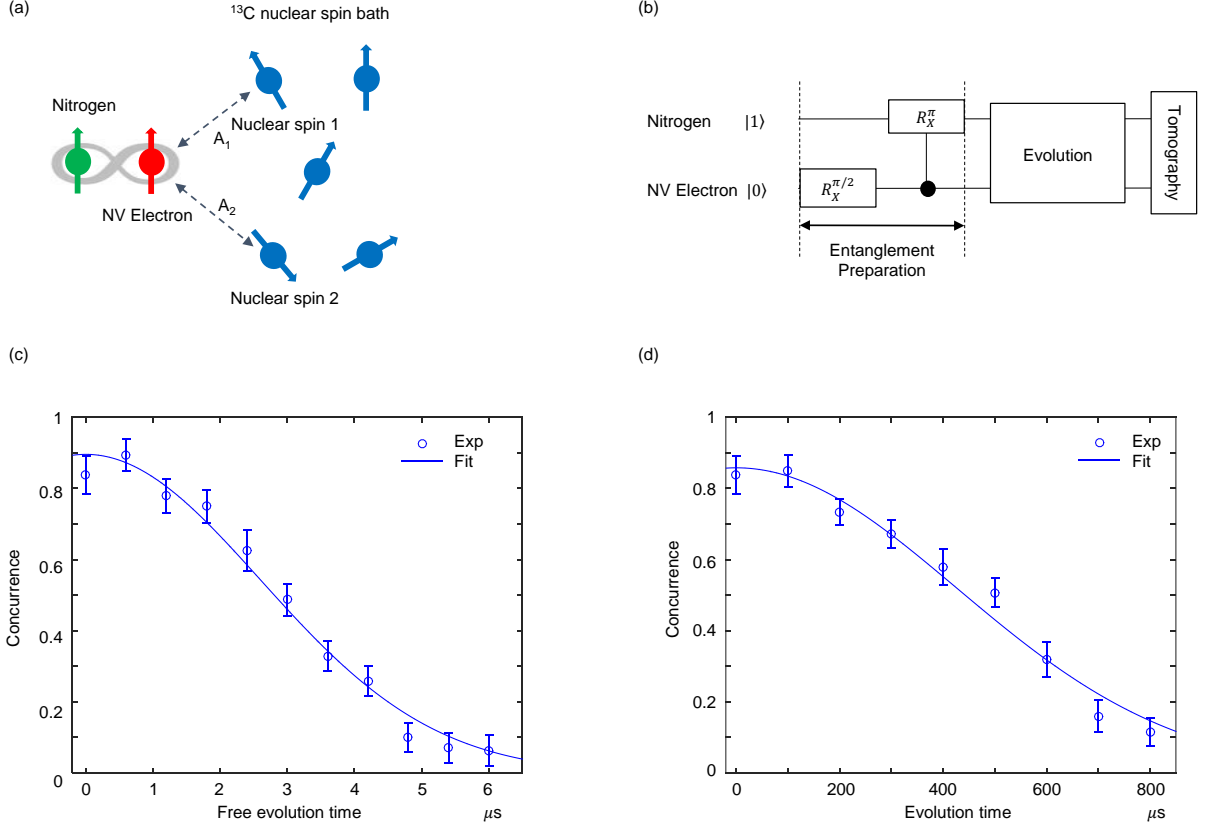


FIG. 1: Experimental system. (a) The NV electron spin (red), the host nitrogen nuclear spin (green) and the coupled ^{13}C spin bath (Blue). Entangled state is prepared on the electron-nitrogen pair and is exposed to the spin bath. Hyperfine parameters of distinct carbons are denoted as \mathbf{A}_i for carbon i . (b) Gate sequence to prepare entanglement in the electron-nitrogen nuclear spin pair. The conditional π rotation is implemented by a 2.928 MHz radio-frequency (rf) signal with two fast π rotations of the electron spin symmetric on both sides to protect the coherence of the electron spin. (c) Entanglement decay as a function of free evolution time with the system subject to the fluctuating spin bath. (d) Entanglement decay as a function of evolution time under the Hahn echo. Solid lines are fits by the function $\exp(-(t/T_c)^2)$ with $T_c = 3.7 \mu\text{s}$ ($602 \mu\text{s}$) for Fig. c (Fig. d). The error bars in this and the following figures denote one standard deviation.

protected by two fast π rotations symmetric on both sides of the rf pulse with the form $\tau_1 - \pi - 2\tau_1 - \pi - \tau_1$, where $2\tau_1$ is the rf pulse duration. Final state density matrix is reconstructed from measurements by two-bit state tomography [29].

Entanglement for a two-qubit state ρ can be quantified by concurrence C [30], which is given by $C = \max\{0, \Gamma\}$ where $\Gamma = \sqrt{\lambda_1} - \sqrt{\lambda_2} - \sqrt{\lambda_3} - \sqrt{\lambda_4}$ with λ_i denoting the eigenvalues of the matrix $\rho(\sigma_y \otimes \sigma_y)\rho^*(\sigma_y \otimes \sigma_y)$ in decreasing order, and ρ^* denoting the complex conjugate of ρ in the computational basis $\{|00\rangle, |01\rangle, |10\rangle, |11\rangle\}$. This quantity can be interpreted as a measure for the quantum correlation present in the system and takes the value from 0 to 1.

We start by studying the dynamics of entanglement under free evolution of the two spins. Under this condition, the electron spin is subject to fast decoherence noise induced by the bath. Therefore, asymptotic decay of entanglement is observed by fitting the concurrence to $\exp(-(t/T_c)^2)$ (Fig. 1(c)), where T_c is the electron spin coherence time. A Hahn echo can cancel part of the interaction with the spin bath and thus significantly increase the coherence time. As a result, the observed decay of entanglement under the Hahn echo is also asymptotic but with a much slower decay rate as shown in Fig. 1(d).

A more complicated behavior of entanglement dynamics can be observed if one extends the Hahn echo to periodic repetitions of the Carr-Purcell-Meiboom-Gill (CPMG) sequence (Fig. 2(a)). The CPMG sequence acts as a filter of the bath in the frequency domain, whose center frequency can be tuned by changing the inter-pulse duration 2τ . In experiments we selectively apply four specific filters to the system by choosing corresponding τ and monitor the evolution of entanglement by gradually increasing the number of pulses N (and therefore the total evolution time). Three distinct behaviors of entanglement dynamics are observed: (i) asymptotic decay with $\tau = 2 \mu\text{s}$ (Fig. 2(b)), (ii)

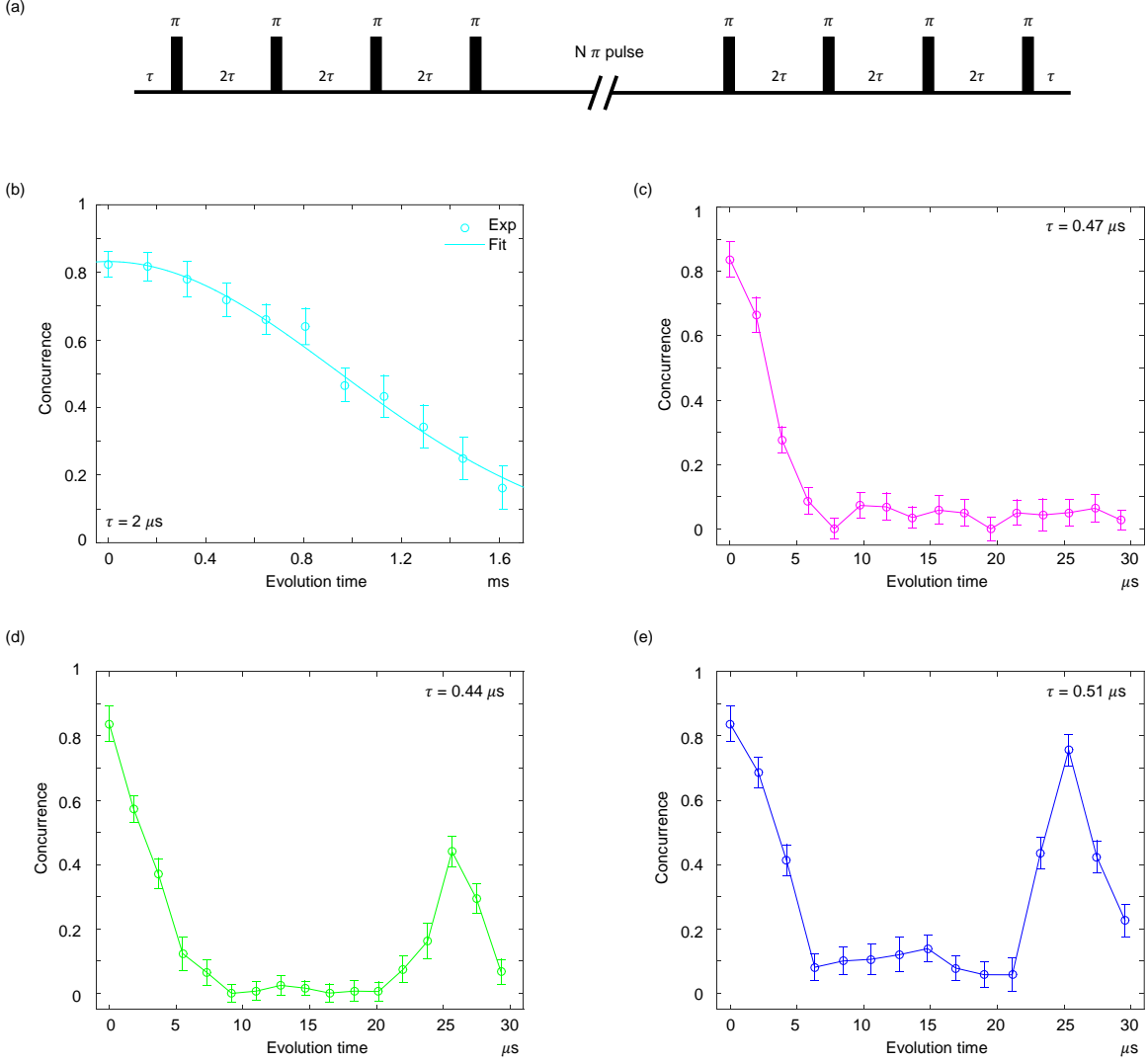


FIG. 2: Decay of electron-nuclear spin entanglement under CPMG sequences. (a) Diagram of the CPMG sequence. (b) Asymptotic decay of entanglement as a function of the total evolution time at $\tau = 2 \mu\text{s}$. Solid line is a fit by the function $\exp(-(t/T_2)^2)$ with $T_2 = 1.33 \text{ ms}$. (c) Observation of entanglement sudden death as a function of the evolution time at $\tau = 0.47 \mu\text{s}$. (d, e) Non-Markovian entanglement dynamics as a function of the total evolution time at $\tau = 0.44 \mu\text{s}$ and $\tau = 0.51 \mu\text{s}$, which shows entanglement sudden death and rebirth.

entanglement sudden death with $\tau = 0.47 \mu\text{s}$ (Fig. 2(c)), (iii) non-Markovian behavior which shows entanglement sudden death and rebirth with $\tau = 0.44 \mu\text{s}$ and $\tau = 0.51 \mu\text{s}$ (Fig. 2(d,e)).

The phenomena can be explained by the spectral filtering of the spin bath through the CPMG sequence, which either suppresses [31–33] or resonantly amplifies [34] the interactions of the electron spin with the structured bath. The power spectrum $S(\omega)$ of the bath includes two parts [35]: thermal noise due to the random orientations and flip-flops of the bath spins at room temperature, and dynamical quantum noise caused by the evolution of nuclear spins. Under the CPMG sequence, both components of the surrounding bath can be detected by measuring the coherence decay $W(t)$ of the electron spin [36, 37]

$$W(t) = \exp[-\chi(t)] = \exp \left[- \int_0^\infty \frac{d\omega}{\pi} \frac{S(\omega)}{\omega^2} F_N(\omega t) \right] \quad (1)$$

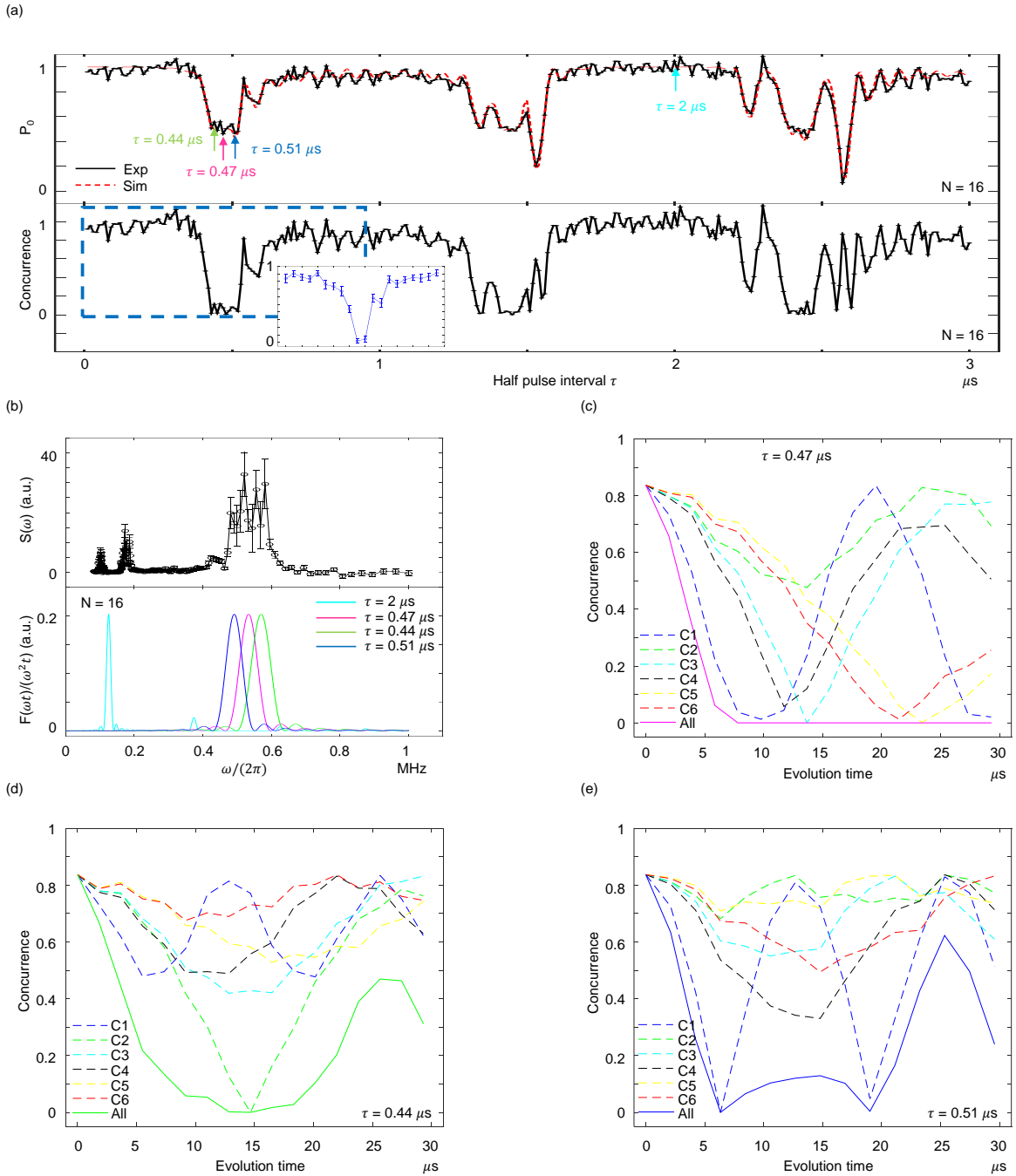


FIG. 3: Analysis of the entanglement evolution under CPMG sequences. (a) Upper panel: decay of electron coherence as a function of half inter-pulse duration τ with $N = 16$. Black dots and solid line are experimental data taken every 10 ns. Red dashed line denotes the simulation result under six identified carbon nuclear spins in the bath with their hyperfine parameters calibrated by the method described in the supplementary material [40]. Arrows indicate corresponding τ in Fig. 2(b,c,d,e) respectively. Lower panel: calculated entanglement concurrence from electron coherence in the upper figure. Inset: experimental results with the same time range in the blue dashed square. Blue circles are experimental data taken every 50 ns. (b) Upper panel: noise spectrum constructed from electron spin coherence in Fig. 3(a). Central components correspond to the first order resonance of the nuclear spin bath. Higher order resonance terms are shown as peaks at lower frequencies. Lower panel: filter function of the CPMG sequences with $N = 16$. Peaks appear at $\omega_0/(2\pi) = 1/(4\tau)$. (c,d,e) Simulation of entanglement decay under the same condition described in Fig. 2(c,d,e) respectively. Dashed lines are results corresponds to single identified carbon nuclear spin. Solid line is the result with effects of six carbon nuclear spins combined together.

where

$$F_N(\omega t) = 8 \sin^2\left(\frac{\omega t}{2}\right) \frac{\sin^4\left(\frac{\omega t}{4N}\right)}{\cos^2\left(\frac{\omega t}{2N}\right)} \quad (2)$$

is the filter function [38] associated with the pulse number N and the total evolution time $t = 2N\tau$ of the CPMG sequence. The detected probability corresponds to $P_0 = (1/2)(W(t) + 1)$.

We focus on the dynamical quantum noise of the bath, as the effects of static thermal noise are removed by the CPMG sequence. According to equation (1), the precession of the ^{13}C spin bath produces a coherence dip of electron spin centered at the nuclear Larmor frequency $\omega_L = \gamma_C B_z$, where γ_C is the nuclear spin gyromagnetic ratio and B_z is the external magnetic field. Due to the frequency shift caused by the hyperfine interactions of multiple nuclear spins in the bath, the observed signal is shown as a broad collapse instead of a dip (upper panel of Fig. 3(a)). Higher order resonances of the bath are observed as broadening of the collapses and splitting of isolated dips. The influence of the bath on the electron spin coherence takes effect on the entangled state shared between the electron and the nuclear spin and leads to disruption of entanglement as shown in lower panel of Fig. 3(a), where entanglement concurrence is calculated from the detected P_0 in the upper panel. We experimentally measure the entanglement concurrence around the bath and observe a consistent behavior with the calculation prediction (Inset of Fig. 3(a)).

Spectrum of the dynamical quantum noise can be constructed from the coherence decay of the electron spin under the CPMG sequence with a spectrum decomposition method [36]. As shown in the upper panel of Fig. 3(b), central components in the spectrum correspond to first order resonance of the nuclear spin bath and peaks in the lower frequencies are higher order resonance terms. With fixed inter-pulse duration 2τ , filter function of the CPMG sequence covers a narrow frequency region centered at $\omega_0 = \pi/(2\tau)$ (See lower panel of Fig. 3(b) for filter function). If we control the filter peak to be off resonant from the bath (for example $\tau = 2\mu\text{s}$), bath influence on the electron spin is sufficiently suppressed, thus concurrence of entanglement is shown as Markovian asymptotic decay and can be kept to the limit of electron spin T_2 (Fig. 2(b)). On the contrary, if we control the filter to be on resonant with the bath, interactions of the electron spin with multiple carbons are amplified, leading to information flow between the electron spin and the bath. To understand the mechanism of the information flow, we experimentally identify six carbon nuclear spins in the bath which give strong influence on the electron spin coherence [39] (Fig. 3(a) and Fig. 1 in [40]) and perform simulations with the 8-qubit system [40]. From Fig. 3(c), when the filter amplifies the center of the bath ($\tau = 0.47\mu\text{s}$), information exchanges between the electron spin and several carbons with separate exchange frequency are mixed together and on average are shown as dissipation from the electron spin to the bath. Consequently, entanglement vanishes completely in a finite time and ESD is observed. Comparatively, when the filter amplifies the edge of the bath ($\tau = 0.44\mu\text{s}$ and $\tau = 0.51\mu\text{s}$), information flow is dominant by the interaction of the electron spin with the resonant carbon (C1 with $\tau = 0.44\mu\text{s}$, C2 with $\tau = 0.51\mu\text{s}$), thus revival of entanglement is observed after the concurrence drops to the minimal value (Fig. 3(d,e)). Full revival is prohibited by the interactions with other carbons in the bath.

For the initially entangled states evolving under the CPMG sequence, concurrence coincides with the measure for quantum non-Markovianity of the electron-bath system [21], which in the standard approach is defined by the trace difference between two quantum states $D(\rho_1(t), \rho_2(t)) = (1/2)\|\rho_1(t) - \rho_2(t)\|$, where $\rho_{1,2}(t) = |\phi_{1,2}(t)\rangle\langle\phi_{1,2}(t)|$ and $|\phi_{1,2}(0)\rangle = (1/\sqrt{2})(|0\rangle_e \pm |1\rangle_e)$. Therefore, the observed revival of entanglement also quantifies the memory effect of the system.

To further probe the non-Markovianity of the system, we control the filter to be on resonant with isolated single carbon where influence of the unwanted spin bath is suppressed (Fig. 4(a)). Under this condition, the isolated carbon acts as a register in a way that coherence information flows back and forth between the electron-nuclear pair and the electron-carbon pair, thus leads to entanglement Rabi oscillations. As can be observed from Fig. 4(b,c), after dropping to 0, the concurrence immediately begins to grow and recovers to the initial value after a half cycle. The period of this entanglement Rabi oscillation is dependent on the transverse component of the hyperfine parameters ($A_{xz1} = 114.5(1)\text{kHz}$, $A_{xz2} = 58.7(3)\text{kHz}$).

In summary, beyond demonstrating a perspective insight into the entanglement dynamics, our observations provide a possible method to control entanglement in a hybrid system coupled to a natural reservoir. Moreover, measurement for quantum non-Markovianity allows for the study of memory effects emerging from correlations within the environment.

[1] D. P. DiVincenzo, Fortschr. Phys. 48, 9-11, 771-783 (2000).

[2] C. H. Bennett, and D. P. DiVincenzo, Nature 404, 247 (2000).

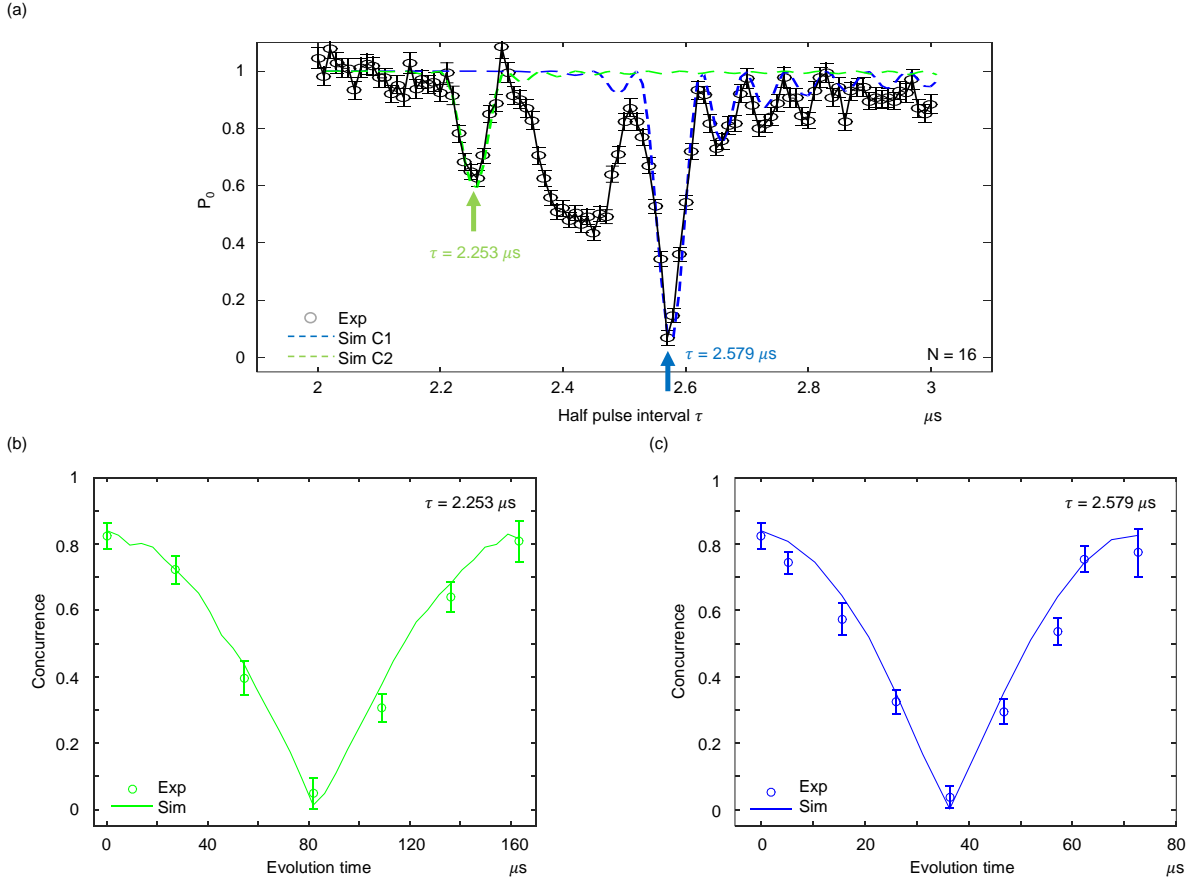


FIG. 4: Decay of electron coherence and electron-nuclear spin entanglement under the CPMG sequences with inter-pulse duration τ on resonant with a single carbon. (a) Decay of electron coherence as a function of half inter-pulse duration τ under CPMG sequences with $N = 16$. Black circles are experimental data taken every 10ns. (b) Entanglement decay as a function of the total evolution time with the half inter-pulse duration $\tau = 2.253 \mu\text{s}$. The sequence is on resonant with carbon 2 (green arrow in Fig. 4(a)). (c) Entanglement decay as a function of the total evolution time with the half inter-pulse duration $\tau = 2.579 \mu\text{s}$. The sequence is on resonant with carbon 1 (blue arrow in Fig. 4(a)). Blue (green) solid lines are simulation results with calibrated parameters for carbon 1 (2).

- [3] H.-J. Briegel, W. Dur, J. I. Cirac, and P. Zoller, Phys. Rev. Lett. 81, 5932 (1998).
- [4] L.-M. Duan, M. D. Lukin, J. I. Cirac, and P. Zoller, Nature (London) 414, 413 (2001).
- [5] W. H. Zurek, Rev. Mod. Phys. 75, 715(2003).
- [6] F. Mintert, A. R. R. Carvalho, M. Kus, A. Buchleitner, Phys. Rep. 415, 207 (2005)
- [7] T. Yu, J. H. Eberly, Phys. Rev. Lett. 93, 140404 (2004).
- [8] T. Yu, J. H. Eberly, Phys. Rev. Lett. 97, 140403 (2006).
- [9] T. Yu, J. H. Eberly, Science 323, 598 (2009).
- [10] L. Diosi, Progressive Decoherence and Total Environmental Disentanglement, Springer Lecture Notes in Physics 622, 2003.
- [11] P. J. Dodd, J. J. Halliwell, Phys. Rev. A 69, 052105 (2004).
- [12] P. Marek, J. Lee, M. S. Kim, Phys. Rev. A 77, 032302 (2008).
- [13] D. Tolkunov, V. Privman, P. K. Aravind, Phys. Rev. A 71, 060308(R) (2005).
- [14] J. P. Paz, A. J. Roncaglia, Phys. Rev. Lett. 100, 220401 (2008).
- [15] C. S. Chou, T. Yu, B. L. Hu, Phys. Rev. E 77, 011112 (2008).
- [16] C. Cormick, J. P. Paz, Phys. Rev. A 78, 012357 (2008).
- [17] C. Y. Lai, J. T. Hung, C. Y. Mou, P. Chen, Phys. Rev. B 77, 205419 (2008).
- [18] A. Abliz, H. J. Gao, X. C. Xie, Y. S. Wu, W. M. Liu, Phys. Rev. A 74, 052105 (2006).
- [19] M. P. Almeida, F. de Melo, M. Hor-Meyll, A. Salles, S. P. Walborn, P. H. Souto Ribeiro and L. Davidovich, Science 316, 579 (2007).
- [20] J.-S. Xu, C.-F. Li, M. Gong, X.-B. Zou, C.-H. Shi, G. Chen, and G.-C. Guo, Phys. Rev. Lett. 104, 100502 (2010).
- [21] B.-H. Liu, L. Li, Y.-F. Huang, C.-F. Li, G.-C. Guo, E.-M. Laine, H.-P. Breuer and J. Piilo, Nature Phys. 7, 931 (2011).
- [22] S. Cialdi, D. Brivio, E. Tesio, and M. G. A. Paris, Phys. Rev. A 83, 042308 (2011).

- [23] B.-H. Liu, D.-Y. Cao, Y.-F. Huang, C.-F. Li, G.-C. Guo, E.-M. Laine, H.-P. Breuer and J. Piilo, *Sci. Rep.* 3, 1781 (2013).
- [24] J. Laurat, K. S. Choi, H. Deng, C. W. Chou, H. J. Kimble, *Phys. Rev. Lett.* 99, 180504 (2007).
- [25] M. M. Wolf, J. Eisert, T. S. Cubitt, and J. I. Cirac, *Phys. Rev. Lett.* 101, 150402 (2008).
- [26] H.-P. Breuer, E.-M. Laine, and J. Piilo, *Phys. Rev. Lett.* 103, 210401 (2009).
- [27] A. Rivas, S. F. Huelga, and M. B. Plenio, *Phys. Rev. Lett.* 105, 050403 (2010).
- [28] V. Jacques, P. Neumann, J. Beck, M. Markham, D. Twitchen, J. Meijer, F. Kaiser, G. Balasubramanian, F. Jelezko, and J. Wrachtrup, *Phys. Rev. Lett.* 102, 057403 (2009).
- [29] C. Zu, W.-B. Wang, L. He, W.-G. Zhang, C.-Y. Dai, F. Wang, and L.-M. Duan, *Nature* 514, 72 (2014).
- [30] W. K. Wootters. *Phys. Rev. Lett.* 80, 2245 (1998).
- [31] G. de Lange, Z. H. Wang, D. Riste, V. V. Dobrovitski, R. Hanson, *Science* 330, 60 (2010).
- [32] C. A. Ryan, J. S. Hodges, and D. G. Cory, *Phys. Rev. Lett.* 105, 200402 (2010).
- [33] F. Wang, C. Zu, L. He, W.-B. Wang, W.-G. Zhang, L.-M. Duan, *Phys. Rev. B* 94, 064304 (2016).
- [34] T. H. Taminiiau, J. J. T. Wagenaar, T. van der Sar, F. Jelezko, V. V. Dobrovitski and R. Hanson, *Phys. Rev. Lett.* 109, 137602 (2012).
- [35] N. Zhao, J.-L. Hu, S.-W. Ho, J. T. K. Wan and R. B. Liu, *Nature Nanotech.* 6, 242-246 (2011).
- [36] N. Bar-Gill, L.M. Pham, C. Belthangady, D. Le Sage, P. Cappellaro, J.R. Maze, M.D. Lukin, A. Yacoby and R. Walsworth, *Nat. Commun.* 3, 858 (2012).
- [37] N. Zhao, J. Honert, B. Schmid, M. Klas, J. Isoya, M. Markham, D. Twitchen, F. Jelezko, R.-B. Liu, H. Fedder and J. Wrachtrup, *Nature Nanotech.* 7, 657-662 (2012).
- [38] L. Cywinski, R. M. Lutchyn, C. P. Nave, and S. Das Sarma, *Phys. Rev. B* 77, 174509 (2008).
- [39] F. Wang, Y.-Y. Huang, Z.-Y. Zhang, C. Zu, P.-Y. Hou, X.-X. Yuan, W.-B. Wang, W.-G. Zhang, L. He, X.-Y. Chang, and L.-M. Duan, *Phys. Rev. B* 96, 134314 (2017).
- [40] Supplementary Material.

Supplementary online material for Observation of entanglement sudden death and rebirth by controlling solid-state spin bath

F. Wang¹, P.-Y. Hou¹, Y.-Y. Huang¹, W.-G. Zhang¹, X.-L. Ouyang¹, X.
Wang¹, X.-Z. Huang¹, H.-L. Zhang¹, L. He¹, X.-Y. Chang¹, L.-M. Duan^{*1,2}

¹*Center for Quantum Information, IIIS, Tsinghua University, Beijing 100084, PR China*

²*Department of Physics, University of Michigan, Ann Arbor, Michigan 48109, USA*

EXPERIMENTAL SETUP AND STATE DETECTION

We use a home-built confocal microscopy system to optically address single NV center in the diamond. Initialization and readout of electron spin associated with single NV center is achieved by a 532 nm green laser controlled by two acoustic optical modulators (AOMs). Both the AOMs are set in a double pass configuration to control the on-off and constrain the leakage of the green laser. After optical mode shaping through a single mode fiber, the green laser is reflected by a wave length dependent Dichroic Mirror (DM) and focused by an oil immersed objective lens onto the bulk diamond sample. The fluorescent photons pass through the same DM mirror and get collected by a single photon detector with a 637 nm long pass filter.

The sample is attached to a cover glass which is mounted on a 3-axis closed-loop piezo. The microwave signal used for manipulation of electron spin is generated by a carrier signal modulated at an IQ mixer by two analog outputs of an Arbitrary Waveform Generator (AWG) and delivered with a waveguide transmission line fabricated on the cover glass. The radio frequency signal for manipulation of nitrogen nuclear spin is generated by another analog channel of the AWG and delivered with a fabricated coplanar coil on a PCB board, which is mounted and detached from the other side of the sample. Both signals are amplified before sent into the sample to achieve reasonable rabi frequencies.

All the experiments are performed at room temperature with at least 10^6 repetitions for measurement of each data point. The electron spin state is calculated with $P_0 = (C_{Signal} - C_{Dark}) / (C_{Bright} - C_{Dark})$ in each experiment cycle, where P_0 is the probability for state $|m_s = 0\rangle$, C_{Signal} is number of photons collected for 300 ns right after the detection laser arises, C_{Bright} and C_{Dark} are number of photons collected for the same period of time with electron spin at $|m_s = 0\rangle$ and $|m_s = -1\rangle$ states separately.

Entanglement measurements are performed by mapping the two-bit information onto the electron spin population as described in Ref [1]. Final state density matrix for the entangled state is extracted from the two-bit tomography result with a maximum likelihood calculation.

NUMERICAL SIMULATION

The numerical simulation is performed in the rotating frame in the eight-qubit system composed of electron spin, nitrogen nuclear spin and six weakly coupled ^{13}C nuclear spins with the Hamiltonian

$$H = \Delta S_z^2 + \gamma_e B_z S_z + \gamma_n B_z I_{nz} + A_{\parallel} S_z I_{nz} + Q I_{nz}^2 + \sum_{k=1}^6 \gamma_c B_z I_{cz}^{(k)} + S_z \sum_{k=1}^6 A_{zz}^{(k)} I_{cz}^{(k)} + S_z \sum_{k=1}^6 A_{xz}^{(k)} I_{cx}^{(k)}$$

Here, S_z and I_{nz} are the spin-1 electron and nitrogen nuclear spin operator and $I_{cx}^{(k)}$ is the spin-1/2 nuclear spin operator for the k th carbon. Also, $\Delta = 2.87$ GHz denotes the zero field splitting of the electron spin and $Q = -4.945$ MHz denotes the quadrupolar interaction of the nitrogen nuclear spin. Gyromagnetic ratios of electron, nitrogen and carbon nuclear spin are represented with $\gamma_e = 2.8$ MHz/G, $\gamma_n = -0.308$ kHz/G and $\gamma_c = -1.07$ kHz/G respectively. Hyperfine interactions are represented with $A_{\parallel} = -2.162$ MHz for parallel component of the nitrogen nuclear spin and $A_{zz}^{(k)}$ for the parallel (transverse) component of the k th carbon nuclear spin. Magnetic field is set at $B_z = 479$ Gauss. We assume no interactions between the nuclear spins and a noiseless environment without decoherence and relaxation.

* To whom correspondence should be addressed. E-mail: lmduan@umich.edu.

The hyperfine parameters of weakly coupled carbons are first calibrated by fitting the experimental data on the measured electronic spin coherence after the CPMG sequence to the numerical simulation of the corresponding dynamics with the fitting parameters A_{zz} and A_{xz} . Afterwards, carbon 1 and 2 are further calibrated using the nuclear ODMR based method described in Ref [2] to a resolution of 0.05 kHz in A_{zz} and 0.5 kHz in A_{xz} . Hyperfine parameters of other carbons remain at a lower resolution because of the relative long time (compared to the electron coherence time) to initialize the target nuclear spin evolved in the nuclear ODMR method. See Table 1 for the calibrated hyperfine parameters. The resolved six carbons in the bath have the dominant influence on the electron spin coherence dynamics (Fig. 1). Influence of other carbons with smaller A_{xz} are ignored in the simulation, and they have small influence on the experimental data.

Carbon	$A_{zz}(\text{kHz})$	$A_{xz}(\text{kHz})$
1	-77.02(3)	114.5(1)
2	71.03(3)	58.7(3)
3	4(1)	57(7)
4	-13.9(8)	65(4)
5	16(5)	37(9)
6	-20(3)	41(10)

TABLE I: Hyperfine parameters for the six carbons. A_{zz} is the parallel component and A_{xz} is the transverse component. The number in the parenthesis denotes uncertainty in the last digit.

-
- [1] C. Zu, W.-B. Wang, L. He, W.-G. Zhang, C.-Y. Dai, F. Wang, and L.-M. Duan, Nature 514, 72 (2014).
[2] F. Wang, Y.-Y. Huang, Z.-Y. Zhang, C. Zu, P.-Y. Hou, X.-X. Yuan, W.-B. Wang, W.-G. Zhang, L. He, X.-Y. Chang, and L.-M. Duan, Phys. Rev. B 96, 134314 (2017).

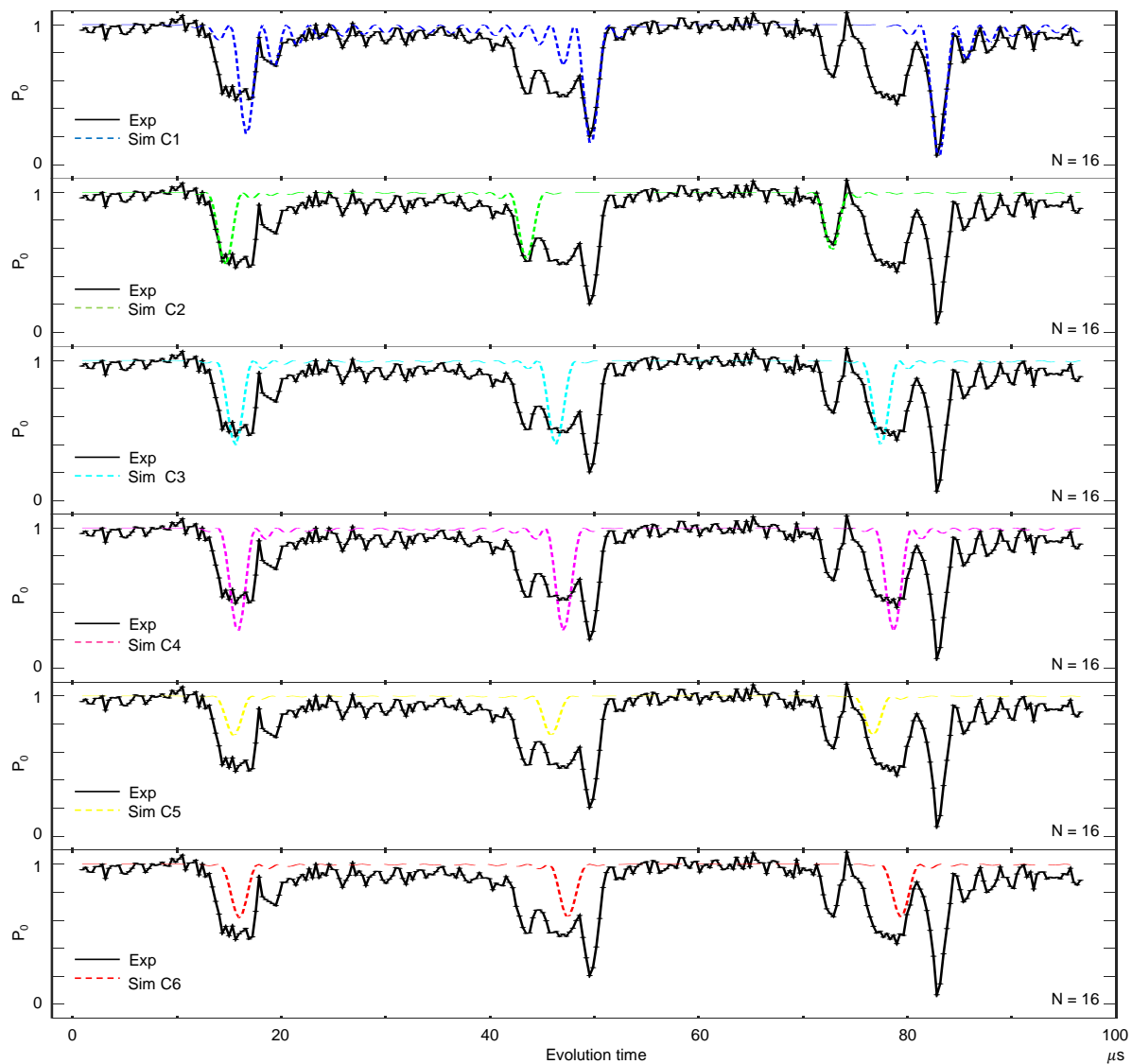


FIG. 1: Coherence of electron spin under CPMG sequences. Black dots and lines are experimental data taken every 10 ns. Dashed lines are simulation results with single carbons respectively.